2025 23rd European Control Conference (ECC)
June 24-27, 2025. Thessaloniki, Greece

A multi-agent NI approach to the secondary voltage synchronisation problem of AC microgrid with controller performance comparison

Salam Athoibi Devi, Parijat Bhowmick, Adino Worku Ayele, and Alexander Lanzon, *Senior Member, IEEE*

***Abstract*— This research study devises a new dynamic output feedback cooperative control scheme relying on the Negative Imaginary (NI) toolkit to address the *secondary voltage synchronisation* issue of the inverter-based Distributed Generating Units (DGUs) that constitute an AC microgrid. Each DGU can be modelled by a nonlinear descriptor system, which, upon being feedback-linearised, gives a double integrator map from the auxiliary input (q_i) to the d-component of the output voltage (v_{od_i}). As a double integrator dynamics intrinsically exhibits the NI property, the feedback-linearised DGUs connected via a network manifest the multi-agent NI property. Therefore, a distributed Strictly NI (SNI) control law can achieve the desired voltage synchronisation among the DGUs of a microgrid. The proof of consensus invokes the *Eigenvalue Loci* technique, for which a complicated Lyapunov theory-based derivation is not necessary. The scheme is resilient to bounded disturbances and variation in the interaction topology and can handle plug-and-play operations. The paper also examines the performance of various first-order and second-order distributed SNI controllers in achieving the desired voltage consensus.**

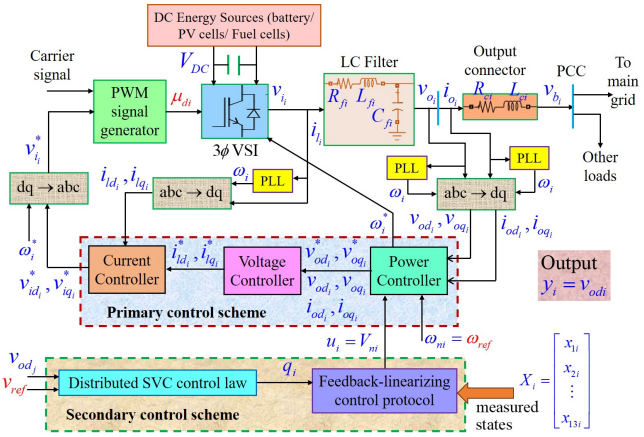

Fig. 1. Architecture of an inverter-based distributed generating unit (DGU) including primary and secondary controller blocks.

I. Introduction

The utility of AC microgrid(s) has been continuously increasing to meet the ever-rising power demand across the globe, especially in the developed and developing countries. Microgrid(s) can be a good option to aid the main grid supply the peak load of a region and to compensate for the shortage of generation capacity of the main generating plant when the power demand of a region exceeds much of the forecasted demand. The main challenge in implementing a microgrid in practice is how to ensure the voltage and frequency synchronisation among the generating units (called DGUs) and with the main grid and how to preserve the stability of the whole microgrid subject to large disturbances, unplanned outages, uncertain loading conditions, etc. In that context, primary and secondary control problem of ac microgrid(s) have received utmost attention over the past two decades. With the prevalence of distributed control methodologies, multi-agent theory and cooperative control, the conventional centralized microgrid control schemes gradually started migrating to decentralized/distributed mode. The literature [1]–[3] did the foundation work in developing a distributed secondary voltage and frequency control scheme for AC microgrid(s) using a multi-agent approach. Since 2014 onwards, this research area has witnessed immense growth and in different directions, for instance, [4]–[8] are some recent literature on this topic. Of late, Negative Imaginary (NI) systems theory is being applied to design dynamic output feedback cooperative control schemes for a variety of homogeneous and heterogeneous multi-agent systems [9]–[18]. The NI theory came into the robust control literature in 2007–08, motivated by the vibration control of flexible structure systems (e.g. cantilever beams, large spacecraft) using positive position feedback [19]. During the last sixteen years, NI theory has continuously flourished and been enriched with substantial theoretical and applied research contributions (see [20], [21] and the references cited therein).

NI theory-based cooperative control techniques have drawn attention because the cumulative motion or activities of various engineering systems (e.g. two-wheeled mobile robots, UAVs, vehicle platoon, mobile sensor networks, etc.) and nature swarms can be approximated or modelled (via feedback linearisation) by a fleet of $\frac{1}{s}$, $\frac{1}{s^2}$ or $\frac{\omega_{ni}^2}{s^2+2\zeta_i\omega_{ni}+\omega_{ni}^2}$ agents (or their combinations) that intrinsically satisfy the NI property. Hence, a simple first- or second-order distributed SNI control law can ensure closed-loop stability and achieve the cooperative control objectives. One of the major advantages of NI-based cooperative control is that the closed-loop stability depends primarily on the sign definiteness of the controller DC gain. One can conveniently construct a

This work was supported by the Engineering and Physical Sciences Research Council (EPSRC) [grant number EP/R008876/1] and the Anusandhan National Research Foundation (ANRF), DST, India [grant numbers SRG/2022/000892 and CRG/2022/006114]. All research data supporting this publication are directly available within this publication. For the purpose of open access, the authors have applied a Creative Commons Attribution (CC BY) licence to any Author Accepted Manuscript version arising.

S. A. Devi, Dr P. Bhowmick and A. W. Ayele belong to the EEE Department of IIT Guwahati, Assam–781039, India. Prof A. Lanzon is with the Control Systems Centre, Department of EEE, School of Engineering, University of Manchester, UK. Emails: {d.salam, parijat.bhowmick, a.adino}@iitg.ac.in, Alexander.Lanzon@manchester.ac.uk.

family of feasible SNI controllers by exploiting this condition without applying a formal cooperative controller synthesis algorithm. The pioneering research on this topic was published in [9] and [10], which were later followed by [22], [11], [17], etc., to develop NI-based formation control schemes for multi-UGV and multi-UAV systems. In a contemporary time, [12] adopted the Eigenvalue Loci technique from [23] to establish the leader-following consensus control of single-integrator robotic (being NI) agents without applying the results of [9] and [10]. The results of [12] were extended to a more general class of multi-agent NI systems to achieve formation control of ground robots [22], quadcopters [14], [15], tricopters [18], platooning of trains [13], etc.

This paper proposes an NI theory-based dynamic output feedback cooperative control scheme to solve the distributed secondary voltage control (DSVC) problem of an AC microgrid. As the DGUs are not identical and the dynamics of the DGUs are highly nonlinear and coupled, an input-output feedback linearisation technique is first applied to obtain a reduced-order linear mapping ($\frac{1}{s^2} : q_i \mapsto v_{od_i}$ in Fig. 1) of the voltage dynamics and ensure internal stability of the overall DGU. In essence, it devises a two-layer (or two-loop) cooperative control scheme, as shown in Fig. 3. The theoretical proof of consensus exploits the Eigenvalue Loci technique instead of the commonly used Lyapunov stability-based approaches, thereby avoiding highly complicated lines of proof. The proposed scheme facilitates the plug-and-play operation (i.e. sudden disconnection and connection of some units) and topology switching without any modifications or improvements of the control law. Unlike most other literature on NI-based cooperative control [9]–[15], [17], this paper explores several feasible controller configurations and compares them based on the steady-state and dynamic performance of the consensus achieved under their actions.

Notation and symbols: Most of the notations and symbols are standard. $\lambda_i[A]$ denotes the i^{th} eigenvalue of a square matrix $A \in \mathbb{C}^{n\times n}$. A^* denotes the complex conjugate transpose of $A \in \mathbb{C}^{n\times n}$. $\Re[z]$ and $\Im[z]$ denote respectively the real and imaginary parts of a complex variable $z \in \mathbb{C}$. The Kronecker product of two matrices A and B is denoted by $A \otimes B$. I_n denotes an n^{th}-order Identity matrix and $\mathbf{1}_n$ denotes an $n \times 1$ vector with all 1s. $\text{diag}\{a_1, a_2, \cdots, a_n\}$ represent an $n \times n$ diagonal matrix with the diagonal entries $a_i\ \forall i \in \{1, 2, \ldots, n\}$. The set of all $m \times n$ real, rational, proper transfer function matrices with no poles in the open RHP is denoted by $\mathscr{R}^{m\times n}$, whereas $\mathscr{RH}_\infty^{m\times n}$ is a strict subset of $\mathscr{R}^{m\times n}$ that consists of only asymptotically stable transfer function matrices.

II. Essential Prerequisites and Problem Formulation

A. Definitions of NI and SNI systems

The prerequisite section begins with the definitions of NI and SNI transfer functions.

Definition 1: (**NI System**) [24], [25] A system $\Xi(s) \in \mathscr{R}^{m\times m}$ is NI if $j[\Xi(j\omega) - \Xi(j\omega)^*] \geq 0\ \forall\omega \in (0, \infty)$ except those $\omega_0 \in \omega$ where $s = j\omega_0$ is a pole of $\Xi(s)$. If $\omega_0 \in (0, \infty)$, the multiplicity of the pole $(s^2 + \omega_0^2)$ cannot be more than one and the residue matrix $\Delta|_{s=j\omega_0} \triangleq \lim_{s\to j\omega_0}(s - j\omega_0)j\Xi(s) = \Delta|^*_{s=j\omega_0} \geq 0$. If $s = 0$ is a pole of $\Xi(s)$, then $\lim_{s\to 0} s^k\Xi(s) = 0\ \forall k \geq 3$ and the residue matrix $\Delta|_{s=0} \triangleq \lim_{s\to 0} s^2\Xi(s)\Delta|^*_{s=0} \geq 0$.

Definition 2: (**SNI System**) [19], [25] A system $\Xi(s) \in \mathscr{RH}_\infty^{m\times m}$ is SNI if $j[\Xi(j\omega) - \Xi(j\omega)^*] > 0\ \forall\omega \in (0, \infty)$.

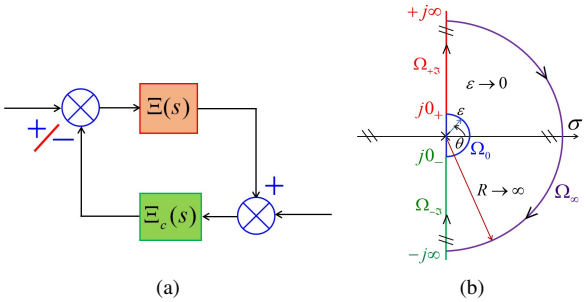

(a) (b)

Fig. 2. (a) A feedback interconnection of two square LTI systems $\Xi(s)$ and $\Xi_c(s)$; (b) The classical $\mathscr{D}$ contour to cover the entire closed right half of the s-plane for the systems having poles at the origin.

B. Properties of multi-agent NI systems

Consider a multi-agent Negative Imaginary (NI-MAS) system consisting of N agents. The interactions among the agents is modelled by an algebraic graph $\mathscr{G}$ characterised by the Laplacian matrix $\mathscr{L} = \mathscr{D} - \mathscr{A}$ where $\mathscr{D}$ and $\mathscr{A}$ denote respectively the in-degree matrix and adjacency matrix. In this study, we will assume that the graphs satisfy the following property.

Property 1: The graph $\mathscr{G}$ is connected when bidirected and contains at least one directed spanning tree when directed. In the case of a directed graph, it must have a root node (also called the 'leader' or 'target'), which has a directed path to every other nodes.

Under the *spanning tree* assumption, $\mathscr{L}$ satisfies the properties of an $\mathscr{M}$-matrix [26]. For directed graphs, $\Re\{\lambda_i[\mathscr{L}]\} \geq 0\ \forall i \in \{1, 2, \ldots, N\}$ and for bidirected (or bidirected) graphs, $\mathscr{L} = \mathscr{L}^\top \geq 0$. Furthermore, for both directed and bidirected graphs, $\mathscr{L}$ is a singular and irreducible $\mathscr{M}$-matrix with $\text{rank}[L] = N - 1$.

We define $\mathbb{P} = \text{diag}\{p_1, p_2, \cdots, p_N\}$ as the pinning-gain matrix where the elements $p_i = 0$ or 1, for $i \in \{1, 2, \ldots, N\}$, decides whether or not the i^{th} node is connected to the root node (labelled as '0'). Owing to Property 1, at least one p_i must be non-zero. Under this condition, $\mathscr{L} + \mathbb{P}$ becomes a non-singular and irreducible $\mathscr{M}$-matrix. For directed graphs, $\Re\{\lambda_i[\mathscr{L} + \mathbb{P}]\} > 0\ \forall i \in \{1, 2, \ldots, N\}$ and for bidirected cases, $(\mathscr{L} + \mathbb{P}) = (\mathscr{L} + \mathbb{P})^\top > 0$. Lemma 1, given below, states that a fleet of NI/SNI agents connected via a bidirected graph retains the NI/SNI property, called the multi-agent NI/SNI property.

Lemma 1: [9], [12] Let $\Xi(s)$ be an NI (resp. SNI) system and N such systems connected by a bidirected graph $\mathscr{G}$ form a multi-agent system characterised by the transfer function

mapping $\tilde{\Xi}(s) = (\mathscr{L} + \mathbb{P}) \otimes \Xi(s)$. Let $\mathscr{G}$ satisfy Property 1. Then, $\bar{M}(s)$ retains the NI (resp. SNI) property. The converse is also true.

C. Eigenvalue loci theory

The Eigenvalue Loci technique, developed by MacFarlane and Belletrutti between 1969–1973, extends the concepts of the Nyquist plot and the associated stability criteria to MIMO LTI systems. The eigenvalue loci of an $n \times n$ real, rational, proper transfer function matrix $\Xi(s)$, denoted by $\gamma_i(s)$ where $i \in \{1, 2, \ldots, n\}$, is essentially a conformal mapping of $\det[\Xi(s)]$ from the s-plane to the eigenvalue loci plane when the complex frequency s takes on the values from the $\mathscr{D}$-contour shown in Fig. 2b indented around the origin to avoid the poles at $s = 0$ (if any). Theorem 1 given below states how the counter-clockwise encirclements of all $\gamma_i(s)$ of a loop transfer function mapping $\Xi_L(s) \triangleq \Xi(s)\Xi_c(s)$ of an interconnection (Fig. 2a) determines the closed-loop stability.

Theorem 1: [27], [28] Consider a feedback interconnection of two square, finite-dimensional, MIMO LTI systems $\Xi(s)$ and $\Xi_c(s)$ as shown in Fig. 2a. Suppose the loop is well-posed and there is no pole-zero cancellation on the closed right-half plane while forming the loop. The closed-loop system remains asymptotically stable if the total number of counter-clockwise encirclements of the critical point made by all the eigenvalue loci $\gamma_i(j\omega)$ of the loop transfer function matrix $\Xi_L(s) \triangleq \Xi(s)\Xi_c(s)$ equals to the number of the unstable (i.e. open right-half plane) poles of $\Xi_L(s)$. Note that for a negative feedback interconnection, the critical point is $(-1 + j0)$; while for positive feedback cases, it becomes $(1 + j0)$.

D. Problem formation

This paper designs a two-layer (or two-loop) distributed dynamic output feedback cooperative control scheme (Fig. 3) to achieve voltage synchronization among the DGUs of an AC microgrid connected via a network. The inner layer applies an appropriate input feedback linearisation scheme to ensure internal stability and simplify the voltage dynamics ($q_i \mapsto v_{od_i}$) into a double integrator system under some constraints. While the outer layer implements an NI-based distributed output feedback control law on the feedback-linearised DGUs to achieve the voltage synchronization among the DGUs (within a microgrid).

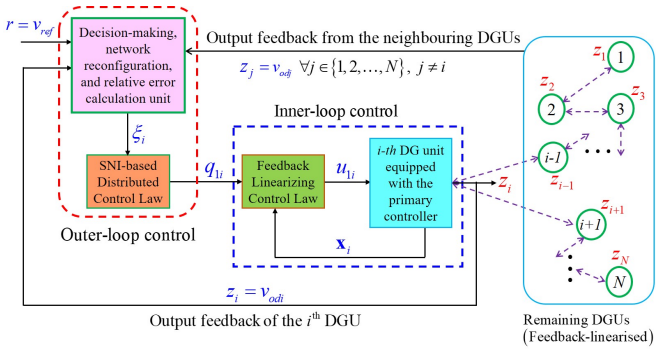

Fig. 3. An NI-based two-layer DSVC scheme with feedback linearisation.

III. Large-signal model of an inverter-based DGU and its feedback linearisation

The architecture of an inverter-based DGU and its large-signal modelling have been adopted from [29], [1] and [3] but with some modifications, improvements in the presentation and corrections in the feedback linearisation portion (given later in this section). Fig. 1 shows a detailed functional block diagram of an inverter-based DGU. The figure also shows the primary and secondary control blocks. The voltage and frequency droop characteristics considered in the primary controller design are given by

$$\begin{cases} \omega_i^* = \omega_{ni} - M_{P_i} P_i, \\ |v_{oi}^*| = v_{od_i}^* = V_{ni} - N_{Q_i} Q_i, \\ v_{oq_i}^* = 0. \end{cases} \tag{1}$$

The following set of nonlinear state-space equations describes the large-signal model of an inverter-based DG unit equipped with the primary control scheme comprised of a sequence of power, voltage and current controllers as illustrated in Fig 1.

$$\begin{aligned}
\dot{x}_{1i} &= \omega_i^* - d_{1i} = -M_{P_i}\, x_{2i} + u_{2i} - d_{1i}, \\
\dot{x}_{2i} &= -\omega_{ci}\, x_{2i} + \omega_{ci}\, x_{10i}\, x_{12i} + \omega_{ci}\, x_{11i}\, x_{13i}, \\
\dot{x}_{3i} &= -\omega_{ci}\, x_{3i} + \omega_{ci}\, x_{11i}\, x_{12i} - \omega_{ci}\, x_{10i}\, x_{13i}, \\
\dot{x}_{4i} &= x_{10i}^* - x_{10i} = -N_{Q_i}\, x_{3i} - x_{10i} + u_i, \\
&\quad [\text{since } x_{10i}^* = v_{od_i}^* = V_{ni} - N_{Q_i} Q_i = u_i - N_{Q_i} x_{3i}] \\
\dot{x}_{5i} &= x_{11i}^* - x_{11i} = -x_{11i}, \quad [\text{since } x_{11i}^* = v_{oq_i}^* = 0] \\
\dot{x}_{6i} &= x_{8i}^* - x_{8i}, \\
\dot{x}_{7i} &= x_{9i}^* - x_{9i}, \\
x_{8i}^* &= F_i\, x_{12i} - \omega_b\, C_{f_i}\, x_{11i} + K_{P_i}^V (x_{10i}^* - x_{10i}) + K_{I_i}^V\, x_{4i}, \\
x_{9i}^* &= F_i\, x_{13i} + \omega_b\, C_{f_i}\, x_{10i} + K_{P_i}^V (x_{11i}^* - x_{11i}) + K_{I_i}^V\, x_{5i}, \\
\dot{x}_{8i} &= -\frac{R_{f_i}}{L_{f_i}} x_{8i} + \omega_i\, x_{9i} + \frac{1}{L_{f_i}} v_{id_i} - \frac{1}{L_{f_i}} x_{10i}, \\
\dot{x}_{9i} &= -\frac{R_{f_i}}{L_{f_i}} x_{9i} - \omega_i\, x_{8i} + \frac{1}{L_{f_i}} v_{iq_i} - \frac{1}{L_{f_i}} x_{11i}, \\
v_{id_i}^* &= -\omega_b\, L_{f_i}\, x_{9i} + K_{P_i}^C (x_{8i}^* - x_{8i}) + K_{I_i}^C\, x_{6i}, \\
v_{iq_i}^* &= \omega_b\, L_{f_i}\, x_{8i} + K_{P_i}^C (x_{9i}^* - x_{9i}) + K_{I_i}^C\, x_{7i}, \\
\dot{x}_{10i} &= \omega_i\, x_{11i} + \frac{1}{C_{f_i}} x_{8i} - \frac{1}{C_{f_i}} x_{12i}, \\
\dot{x}_{11i} &= -\omega_i\, x_{10i} + \frac{1}{C_{f_i}} x_{9i} - \frac{1}{C_{f_i}} x_{13i}, \\
\dot{x}_{12i} &= -\frac{R_{c_i}}{L_{c_i}} x_{12i} + \omega_i\, x_{13i} + \frac{1}{L_{c_i}} x_{10i} - \frac{1}{L_{c_i}} d_{2i}, \\
\dot{x}_{13i} &= -\frac{R_{c_i}}{L_{c_i}} x_{13i} + \omega_i\, x_{12i} + \frac{1}{L_{c_i}} x_{11i} - \frac{1}{L_{c_i}} d_{3i}
\end{aligned}$$

where the states are defined as $x_{1i} \triangleq \delta_i$, $x_{2i} \triangleq P_i$, $x_{3i} \triangleq Q_i$, $x_{4i} \triangleq \phi_{d_i}$, $x_{5i} \triangleq \phi_{q_i}$, $x_{6i} \triangleq \gamma_{d_i}$, $x_{7i} = \gamma_{q_i}$, $x_{8i} \triangleq i_{ld_i}$, $x_{9i} \triangleq i_{lq_i}$, $x_{10i} \triangleq v_{od_i}$, $x_{11i} \triangleq v_{oq_i}$, $x_{12i} \triangleq i_{od_i}$ and $x_{13i} \triangleq i_{oq_i}$; the control input (to the primary control block) is given by $u_i = u_{1i} = V_{ni}$; another control input $u_{2i} = \omega_{ni}$ is maintained constant ($= \omega_{ref}$) when the DSVC is operated without secondary frequency control; the disturbance inputs

are denoted as $d_{1i} = \omega_{com}$, $d_{2i} = v_{bd_i}$ and $d_{3i} = v_{bq_i}$. We can observe that there are thirteen dynamic equations and six algebraic constraints (with respect to $x^*_{8i} = i^*_{ld_i}$, $x^*_{9i} = i^*_{lq_i}$, $x^*_{10i} = v^*_{od_i}$ and $x^*_{11i} = v^*_{oq_i}$, $v^*_{id_i}$ and $v^*_{iq_i}$). It is vital to mention here that v_{id_i} and v_{iq_i} are not considered as states because the dynamics of the VSI has been excluded from the DGU model to reduce its complexity. Hence, the dynamics of a DGU can be expressed by a nonlinear descriptor system

$$E\dot{\mathbf{x}}_i = \mathbf{f}_i(\mathbf{x}_i) + \mathbf{g}_i(\mathbf{x}_i)u_i + \mathbf{k}_i(\mathbf{x}_i)\mathbf{d}_i \tag{3}$$

where $E = \text{diag}\{1,1,1,1,1,1,1,0,0,1,1,0,0,1,1,1,1\} \in \mathbb{R}^{17\times 17}$ and $\mathbf{x}_i = \begin{bmatrix} x_{1i}\ x_{2i}\ \cdots\ x_{7i}\ x^*_{8i}\ x^*_{9i}\ x_{8i}\ x_{9i}\ x^*_{10i}\ x^*_{11i}\ x_{10i}\ \cdots\ x_{13i}\end{bmatrix}^\top$, $u_i = V_{ni}$ and $\mathbf{d}_i = \begin{bmatrix} d_{1i}\ d_{2i}\ d_{3i}\end{bmatrix}^\top$. The mappings $\mathbf{f}_i(\mathbf{x}_i)$, $\mathbf{g}_i(\mathbf{x}_i)$ and $\mathbf{k}_i(\mathbf{x}_i)$ can be easily found after writing all seventeen equations in the vector-matrix format.

To achieve voltage synchronisation among the DGUs of a microgrid depending on the multi-agent systems theory, a nonlinear distributed cooperative control scheme needs to be designed for the DGUs. However, this is a highly challenging task as i) the dynamics of DGUs are highly nonlinear, coupled and of higher order, ii) their dynamics contain both differential equations and algebraic constraints and iii) moreover, the DGUs have structural heterogeneities due to inevitable differences in the line parameters, filters, primary controller parameters, etc. To avoid all these hassles, we seek to find an input-output feedback linearisation technique to get a reduced-order linear mapping of the voltage dynamics (from the auxiliary input q_i to the output v_{od_i}) and to stabilise the internal dynamics of the DGUs. We notice that the $\dot{v}_{od_i} = \dot{x}_{10i}$ equation does not contain any $u_i = V_{ni}$ term. So to establish a link between between V_{ni} and v_{od_i}, we proceed to derive $\ddot{v}_{od_i}$ as detailed below:

$$\begin{aligned}\ddot{v}_{od_i} =& -\left((\omega^*_i)^2 + \frac{1}{C_{f_i}L_{f_i}} + \frac{1}{C_{f_i}L_{c_i}}\right)v_{od_i} + \frac{R_{c_i}}{C_{f_i}L_{c_i}}i_{od_i} \\ &- \frac{2}{C_{f_i}}\omega^*_i i_{oq_i} - \frac{R_{f_i}}{C_{f_i}L_{f_i}}i_{ld_i} + \frac{2}{C_{f_i}}\omega^*_i i_{lq_i} + \frac{1}{C_{f_i}L_{f_i}}v_{id_i} \\ &+ \frac{1}{C_{f_i}L_{f_i}}v_{bd_i} \quad [\text{where } \omega^*_i = \omega_{ni} - m_{P_i}P_i].\end{aligned} \tag{4}$$

From the $i^*_{ld_i} = x^*_{8i}$ algebraic constraint, we find

$$v_{od_i} = v^*_{od_i} - \frac{1}{K^V_{P_i}}\left[i^*_{ld_i} - F_i i_{od_i} + \omega_b C_{f_i} v_{oq_i} - K^V_{I_i}\phi_{d_i}\right] \tag{5}$$

using the relations $v^*_{od_i} = V_{ni} - n_{Q_i}Q_i$ and $\dot{\phi}_{d_i} = v^*_{od_i} - v_{od_i}$ $\forall i \in \{1,2,\ldots,N\}$. Substituting (5) into (4), we obtain the desired relationship

$$\ddot{v}_{od_i} = \alpha_i + \beta_i V_{ni} \tag{6}$$

where $\beta_i = -m_{P_i}\omega_{ci}v_{oq_i}i_{od_i} - \omega^2_{ni} + 2m_{P_i}\omega_{ni}P_i - m^2_{P_i}P^2_i - \frac{1}{L_{f_i}C_{f_i}} - \frac{1}{L_{c_i}C_{f_i}}$ and $\alpha_i = \beta_i - n_{Q_i}Q_i - \frac{1}{K^V_{P_i}}\big(i^*_{ld_i} - F_i i_{od_i} + \omega_b C_{f_i}v_{oq_i} - K^V_{I_i}\phi_{d_i}\big) + \dot{\omega}_{ni}v_{oq_i} + m_{P_i}\omega_{ci}v_{oq_i}P_i - m_{P_i}v^2_{oq_i}i_{oq_i} + \frac{2}{C_{f_i}}\omega_{ni}(i_{lq_i} - i_{oq_i}) + \frac{2}{C_{f_i}}m_{P_i}P_i(i_{oq_i} - i_{lq_i}) - \frac{R_{f_i}}{C_{f_i}L_{f_i}}i_{ld_i} - \frac{1}{C_{f_i}L_{f_i}}v_{id_i} - \frac{R_{c_i}}{L_{c_i}C_{f_i}}i_{od_i} + \frac{1}{L_{c_i}C_{f_i}}v_{bd_i}$. Note that $\dot{\omega}_{ni} = 0$ as $\omega_{ni} = \omega_{ref}$ in the present problem.

We will now construct an auxiliary control law

$$q_i = \alpha_i + \beta_i V_{ni} \quad \forall i \in \{1,2,\ldots,N\} \tag{7}$$

and plugging q_i into (6), we will get $\ddot{v}_{od_i} = q_i$ $\forall i \in \{1,2,\ldots,N\}$. Therefore, $q_i \mapsto v_{od_i}$ gives a double integrator mapping. Define two new state variables $z_{1i} \triangleq v_{od_i} = y_i$ and $z_{2i} \triangleq \dot{v}_{od_i} = \dot{y}_i$, which leads to

$$\dot{z}_i = \begin{bmatrix}0 & 1\\ 0 & 0\end{bmatrix} z_i + \begin{bmatrix}0\\1\end{bmatrix} q_i \qquad \forall i \in \{1,2,\ldots,N\}. \tag{8}$$

The next section will develop a dynamic output feedback cooperative control scheme exploiting the NI property of the feedback-linearised double-integrator agents connected via a bidirected network that intrinsically exhibits the multi-agent NI property.

IV. An NI-based distributed secondary voltage consensus control scheme

This section lays out the fundamental contribution of this paper. It develops a dynamic output feedback cooperative control scheme for the class of multi-agent systems that exhibits the NI/SNI property. In the present scenario, a fleet of feedback-linearised DGUs connected via a bidirected graph leads to a double-integrator MAS, which intrinsically satisfies the NI property with poles at the origin. Hence, a simple first-order or second-order distributed SNI controller with a negative definite DC-gain matrix can achieve asymptotic stability and leader-following consensus (i.e. the voltage synchronisation among the DGUs). The closed-loop stability proof in Theorem 2 extensively relies on the Eigenvalue loci technique [27], [28] and is motived by the developments of [23] and [12].

Theorem 2: Consider an inverter-based DGU equipped with a primary control block, as shown in Fig. 1 and described by the nonlinear descriptor model given in (3). N such DGUs connected via a bidirected topology $\mathscr{G}$ satisfying Property 1 form an AC microgrid. The voltage dynamics of each DG can be simplified to a double integrator system ($q_i \mapsto v_{od_i}$) by applying the feedback linearising control law in (7). Let $\Xi_c(s) \in \mathscr{RH}_\infty$ be an SNI controller with $\Xi_c(0) < 0$ and $k \in (0,\infty)$ be a tuning parameter. Then, the DGUs within the microgrid achieve voltage synchronization by the following SNI-based distributed secondary control law (according to the scheme shown in Fig. 4a)

$$q_i(s) = -k\,\Xi_c(s)\left[\sum_{j=1}^{N} a_{ij}(Y_j(s) - Y_i(s)) + p_i(R(s) - Y_i(s))\right] \tag{9}$$

for all $i \in \{1,2,\ldots,N\}$.
[With a slight abuse of notation, $q_i(s)$ denotes the Laplace transform of the auxiliary control input q_i, as marked in Fig. 1. $R(s)$ is the Laplace transform of the voltage reference v_{ref} and $\mathbf{R}(s) = \mathbf{1}_N \otimes \frac{v_{ref}}{s}$. Note also $y_i = v_{od_i}$ $\forall i$.]

The control law (9) can also be expressed in the compact form $\mathbf{q}(s) = -\big[(\mathscr{L} + \mathbb{P}) \otimes k\,\Xi_c(s)\big]((\mathbf{1}_N \otimes \frac{v_{ref}}{s}) - \mathbf{Y}(s))$.

Proof: The proof proceeds through fulfilling two major objectives: i) To establish the closed-loop asymptotic stability

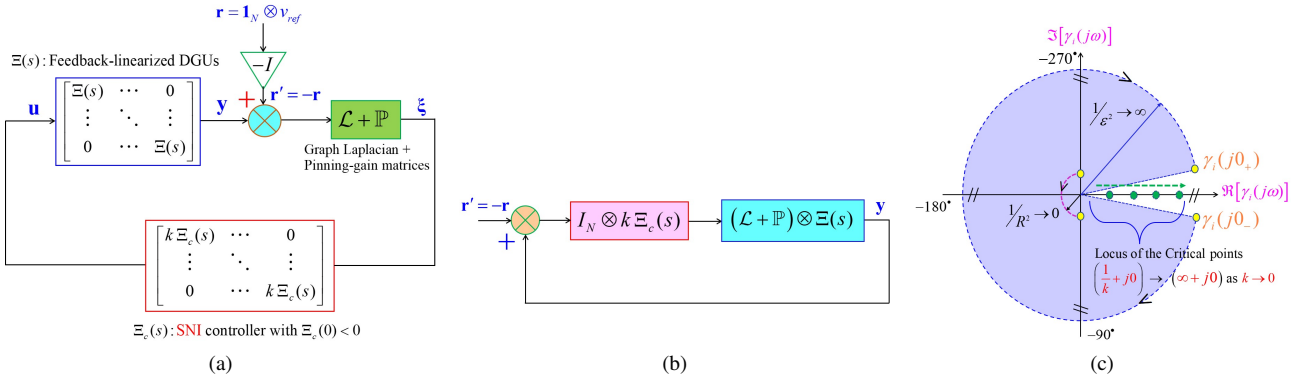

Fig. 4. (a) A positive feedback SNI distributed cooperative control scheme for the feedback-linearised DGUs (given by $\Xi(s) = \frac{1}{s^2}$) connected via a bidirected graph; (b) An equivalent block diagram of the scheme shown in Fig. 4a; (c) All the eigenvalue loci $\gamma_i(s)$ remain within the Purple-coloured region and hence, do not encircle the critical point $(\frac{1}{k} + j0)$ for any $k \in (0, \infty)$.

of the cooperative control scheme shown in Fig. 4a and ii) To show that the consensus tracking error $\xi_i(t) \to 0$ as $t \to \infty$. In the following proof, the notation $\gamma_i(s)$ will represent the eigenvalue loci of the loop transfer function mapping $\Xi_L(s) = (\mathscr{L} + \mathbb{P}) \otimes \Xi(s)\Xi_c(s)$ where $\Xi(s) \triangleq \frac{Y_i(s)}{q_i(s)} = \frac{1}{s^2}$.

Part I: To establish the closed-loop stability of the scheme

We proceed to construct the eigenvalue loci $\gamma_i(s)$ for all $i \in \{1, 2, \ldots, N\}$ of $\Xi_L(s)$ and check the total number of counter-clockwise encirclements of the critical point $(\frac{1}{k} + j0)$ for any value of k in $(0, \infty)$ by all $\gamma_i(s)$ when s traverses along the s-plane $\mathscr{D}$ contour. We define three distinct set of $s \in \mathbb{C}$ which represent the three segments of the s-plane $\mathscr{D}$ contour shown in Fig. 2b.

a) $\Psi_0 \triangleq \{s |\ s = \lim_{\varepsilon \to 0} \varepsilon\, e^{j\theta}, -\frac{\pi}{2} \le \theta \le \frac{\pi}{2}\}$,
b) $\Psi_{\pm\Im} \triangleq \{s |\ s = \pm j\omega, \omega \in (0, \infty)\}$, and
c) $\Psi_\infty \triangleq \{s |\ s = \lim_{R \to \infty} Re^{j\theta}, \frac{\pi}{2} \le \theta \le -\frac{\pi}{2}\}$,

Each eigenvalue locus $\gamma_i(s)$ consists of four segments corresponding to each of the four regions Ψ_0, $\Psi_{+\Im}$, $\Psi_{-\Im}$ and Ψ_∞ of s on the $\mathscr{D}$ contour.

Segment 1: When $s \in \Psi_0$ The first segment of the eigenvalue loci corresponding to $s \in \Psi_0$ is given by

$$\gamma_i(s)|_{s\in\Psi_0} = \lambda_i\left[(\mathscr{L} + \mathbb{P}) \otimes \Xi_c(0)\right] \frac{1}{\varepsilon^2} e^{-j2\theta} \tag{10}$$

for all $i \in \{1, 2, \ldots, N\}$. Since $\Xi_c(0) = \Xi_c(0)^\top < 0$ and $(\mathscr{L} + \mathbb{P}) = (\mathscr{L} + \mathbb{P})^\top > 0$, $\lambda_i[(\mathscr{L} + \mathbb{P}) \otimes \Xi_c(0)]$ can be written as $c_i e^{-j\pi}$ for all $i \in \{1, 2, \ldots, N\}$ where $c_i = |\lambda_i|$. Therefore, $\gamma_i(s)|_{s\in\Psi_0} = \frac{c_i}{\varepsilon^2} e^{-j(\pi+2\theta)}\ \forall i$. It gives $\gamma_i(j0_+)|_{\theta=\frac{\pi}{2}} = \frac{c_i}{\varepsilon^2} e^{-j2\pi} \to +\infty\angle -2\pi$ as $\varepsilon \to 0$. Similarly, $\gamma_i(j0_-)|_{\theta=-\frac{\pi}{2}} = \frac{c_i}{\varepsilon^2} e^{-j0} \to +\infty\angle 0$. As θ varies from $-\frac{\pi}{2}$ to $\frac{\pi}{2}$ on the indent $s \in \Psi_0$, $\angle\gamma_i(s)$ varies from $\frac{\pi}{2}$ to $-\frac{\pi}{2}$. Therefore, every $\gamma_i(s)$ forms a semicircular arc of infinite radius [the Purple-coloured dotted arc in Fig. 4c], starting at $\gamma_i(j0_-)$ terminating at $\gamma_i(j0_+)$ in the clockwise direction. The foregoing analysis reveals that all the eigenvalue loci $\gamma_i(s)$ intersect the negative real axis at infinity because $\gamma_i(j0_+)|_{\theta=0} = \frac{c_i}{\varepsilon^2} e^{-j\pi} \to \infty\angle -\pi$ as $\varepsilon \to 0$. However, none of the $\gamma_i(s)$ intersects the positive real anywhere. Hence, the critical point $(-\frac{1}{k} + j0)$ is never encircled by any of the eigenvalue loci for any $k \in (0, \infty)$.

Segments 2 and 3: When $s \in \Psi_{\pm\Im}$ When $\omega \in (0, \infty)$, that is, $s \in \Psi_{+\Im}$, $\gamma_i(s)$ can be evaluated as

$$\begin{aligned}\gamma_i(s)|_{s\in\Psi_{+\Im}} &= \lambda_i\left[(\mathscr{L} + \mathbb{P}) \otimes \frac{1}{(j\omega)^2}\Xi_c(s)\right] \\ &= \lambda_i\left[(\mathscr{L} + \mathbb{P})\right] \frac{|\Xi_c(j\omega)|}{|(j\omega)^2|}\, e^{j(\phi-\pi)}\end{aligned} \tag{11}$$

for all $i \in \{1, 2, \ldots, N\}$. Since $\phi \in (-\pi, 0)\ \forall\omega \in (0, \omega)$ due to $\Xi_c(s)$ being SNI and $(\mathscr{L} + \mathbb{P}) = (\mathscr{L} + \mathbb{P})^\top > 0$, $\angle\gamma_i(s) = (\phi - \pi) \in (-2\pi, -\pi]\ \forall\omega \in (0, \infty)$, that is, when $s \in \Psi_{+\Im}$. Similarly, $\angle\gamma_i(s) \in [-\pi, 0)\ \forall\omega \in (-\infty, 0)$, that is, when $s \in \Psi_{-\Im}$. Hence, segments 2 and 3 of all the eigenvalue loci corresponding to the regions $s \in \Psi_{+\Im}$ and $s \in \Psi_{-\Im}$ reside in the Purple-coloured region (in Fig. 4c). This ensures that the $\gamma_i(s)$ does not intersect the positive real axis for all i when $s \in \Psi_{\pm\Im}$.

Segment 4: When $s \in \Psi_\infty$ Similar to segment 1, the eigenvalue loci $\gamma_i(s)$ for the segment corresponding to $s \in \Psi_R$ can be expressed as

$$\gamma_i(s)|_{s\in\Psi_\infty} = \lambda_i\left[(\mathscr{L} + \mathbb{P}) \otimes \Xi_c(\infty)\right] \frac{1}{R^2} e^{-j2\theta} \tag{12}$$

for all $i \in \{1, 2, \ldots, N\}$. Since $\Xi_c(0) < 0$, $\angle\gamma_i(s) = -(\pi + 2\theta)$ varies from $-\frac{3\pi}{2}$ to $-\frac{\pi}{2}$ when θ varies from $\frac{\pi}{2}$ to $-\frac{\pi}{2}$ corresponding to $s \in \Psi_\infty$. Therefore, $\gamma_i(+j\infty)|_{\theta=\frac{\pi}{2}} \to 0\angle -\frac{3\pi}{2}$, $\gamma_i(-j\infty)|_{\theta=-\frac{\pi}{2}} \to 0\angle -\frac{\pi}{2}$ and $\gamma_i(\infty + j0)|_{\theta=0} \to 0\angle -\pi$ as $R \to 0$. It signifies that each $\gamma_i(s)$ makes a semicircular arc of infinitesimal radius connecting the points $\gamma_i(+j\infty)$ and $\gamma_i(-j\infty)$ in the counter-clockwise direction (as depicted in Fig. 4a) when $s \in \Psi_\infty$. So, segment 4 also does not intersect the positive real axis.

Each eigenvalue locus $\gamma_i(s)$ of $\Xi_L(s)$ is composed of the four segments introduced above. Fig. 2b indicates that all the eigenvalue loci reside within the Purple-coloured region $\forall s \in \psi_0 \cup \Psi_{\pm j} \cup \Psi_R$. This hence confirms that none of the $\gamma_i(s)$ encircles the critical point $(\frac{1}{k} + j0)$ for any $k \in (0, \infty)$. Finally, Theorem 1 is invoked to conclude that the positive feedback cooperative control scheme depicted in Fig. 4a (equivalently Fig. 4b) remains asymptotically stable under

the conditions $\Xi_c(0) < 0$, $k \in (0, \infty)$ and Property 1 of $\mathscr{G}$.

Part II: To show asymptotic consensus We first denote the consensus error vector as $\xi(t) \triangleq \begin{bmatrix}\xi_1(t) & \cdots & \xi_N(t)\end{bmatrix}^\top$ and obtain the consensus error dynamics $\boldsymbol{\xi}(s) = \big[I_N - (\mathscr{L} + \mathbb{P}) \otimes \frac{k}{s^2}\Xi_c(s)\big]^{-1}\mathbf{R}(s)$ from Fig. 4a where $\mathbf{R}(s) = \mathbf{1}_N \otimes \frac{v_{ref}}{s}$. Now, applying the final value theorem, the steady-state consensus error ξ_{ss} can be derived as

$$\begin{aligned}\xi_{ss} &= \lim_{t\to\infty}\xi(t) = \lim_{s\to 0} s\,\boldsymbol{\xi}(s)\\ &= \lim_{s\to 0} s\Big[I_N - (\mathscr{L}+\mathbb{P})\otimes\frac{k}{s^2}\Xi_c(s)\Big]^{-1}\mathbf{R}(s)\\ &= \lim_{s\to 0} s^3\big[s^2 I_N - (\mathscr{L}+\mathbb{P})\otimes k\,\Xi_c(s)\big]^{-1}\mathbf{R}(s)\\ &= \big[(\mathscr{L}+\mathbb{P})\otimes k\,\Xi_c(0)\big]^{-1}\Big(\lim_{s\to 0} s^2(\mathbf{1}_N\otimes v_{ref})\Big)\\ &= \begin{bmatrix}0 & 0 & \cdots & 0\end{bmatrix}^\top.\end{aligned}$$

Part I and Part II together complete the proof. ■

V. Simulation Studies on a Feedback-Linearised Microgrid Having Four DGUs

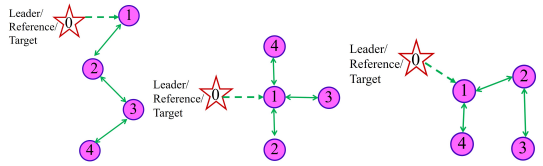

Fig. 5. (a) The interaction topology (leader-following) among the four DGUs where the node (labelled '0') denotes the leader; (b) Topology 2 and c) Topology 3 were considered to test the topology switching.

The case study has considered four agents (the DGUs) connected via a bidirected network, and the 1st agent is connected to the Leader or the Reference node as shown in Fig. 5a. Each node represents the feedback-linearised voltage dynamics $\frac{v_{od_i}(s)}{q_i(s)} = \frac{1}{s^2}$ of the DGU. The main control objective is to achieve an accurate voltage synchronisation among the DGUs; that is, all v_{od_i} should asymptotically follow the v_{ref}. We took $v_{ref} = 440$ V and ω_{ni} was fixed to $\omega_{ref} = 100\pi$ rad/sec $\forall i \in \{1, \ldots, 4\}$ as this paper solves only the DSVC problem.

A. Selection of suitable SNI controller structures via simulation studies

As Theorem 2 suggests, a control designer should first select an SNI controller $\Xi_c(s)$ satisfying $\Xi_c(0) < 0$ and tune the gain parameter $k \in (0, \infty)$ to achieve a decent dynamic performance. So far, most of the literature on NI-based cooperative control has prescribed a first-order SNI controller of the form $\Xi_{c_1}(s) = -\frac{k(s+z_c)}{s+p_c}$ obeying $0 < z_c < p_c$. In this paper, we were curious to examine second-order SNI controllers having two different configurations respectively $\Xi_{c_2}(s) = -\frac{k(s^2+z_{c_1}s+z_{c_0})}{s^2+p_{c_1}s+p_{c_0}}$ satisfying $0 < z_{c_1} < p_{c_1}$ and $\Xi_{c_3}(s) = -\frac{k(s+z_{c_1})(s+z_{c_2})}{(s+p_{c_1})(s+p_{c_2})}$ with $0 < z_{c_1} < p_{c_1} < z_{c_2} < p_{c_2}$.

We designed the following three SNI controllers $\Xi_{c_1}(s) = -\frac{k(s+0.1)}{s+25}$, $\Xi_{c_2}(s) = -\frac{k(s^2+5s+25)}{s^2+4s+38}$ and $\Xi_{c_3}(s) = -\frac{k(s+5)(s+8)}{(s+12)(s+16)}$ via multi-variable root locus technique and selected $k = 3000$ after considerable tuning. Figures 6a–6c show the simulation responses achieved by these three controllers. A comparative study of the controllers given in Table I has been prepared in terms of the transient and steady-state performance. By studying Table I and the simulation responses in Figures 6a–6c, it is evident that $\Xi_{c_1}(s)$ results in lesser %-overshoot (0.07%) compared to $\Xi_{c_2}(s)$ and $\Xi_{c_3}(s)$, which observed a 0.45% overshoot. Although, the difference is really negligible. However, with respect to the steady-state performance, the second-order controllers performed much better than the first-order controller. The % steady-state error in case of $\Xi_{c_1}(s)$ reduced to 6.8×10^{-4} at 25 sec; while $\Xi_{c_2}(s)$ and $\Xi_{c_3}(s)$ took only 6.5 sec and 4.85 sec respectively to attain a % steady-state error of order 10^{-6} and 10^{-10}. The state of asymptotic consensus can be minutely scrutinised by looking into Figures 6d–6f. They reported the magnified version of the v_{od_i} trajectories around their respective settling points in each case. Hence, this comparative study shows that $\Xi_{c_3}(s)$ is the best-performing controller among the three we took. Next, we will examine the performance of $\Xi_{c_3}(s)$ in the presence of external disturbances and subjected to plug-and-play operation and topology switching.

TABLE I. Consensus-reaching performance comparison of the three different DSVC SNI controllers.

Sl. no.	Criteria	$\Xi_{c_1}(s)$	$\Xi_{c_2}(s)$	$\Xi_{c_3}(s)$
1.	% Peak overshoot	0.07 %	0.45 %	0.45 %
2.	Peak time	0.18s	0.2s	0.2s
3.	Steady-state	440.002	440	440
4.	Settling time	25s	6.5s	4.85s
5.	% Steady-state error	6.8×10^{-4}	0 (of order 10^{-6})	0 (of order 10^{-10})

Case 1: Impact of external disturbances

To evaluate the resilience of $\Xi_{c_3}(s)$, a pulse disturbance of two-unit height was injected in the output of each DG (one after another) at different time instants as depicted in Fig. 7a. The figure shows the fluctuations (i.e. the transients) in the v_{od_i} responses during the active period of the disturbance. As the DGUs are interconnected, transients in one inevitably propagate to the others, as revealed in the figure. However, the control action sharply attenuated the transients in each case, and the consensus was reinstated as soon as the disturbance disappeared.

Case 2: Plug and play operation

The plug-and-play operation is one of crucial factors that may lead to prolonged oscillations and even instability. That is why we decided to test the potential of the designed controller to withstand a plug-in or plug-out situation. Fig. 7b portrays a scenario where voltage consensus under healthy condition continued for the first 1.5 seconds. At $t = 1.5$ sec, DGU-4 got disconnected from the network (due to a fault or network issues) causing transients as shown in the magnified view. We observe that the oscillations were within a small range $440.02 - 439.48$ V and decayed sharply to zero within $0.6 - 0.7$ seconds. At $t = 2.5$ sec, DGU-4 rejoined the

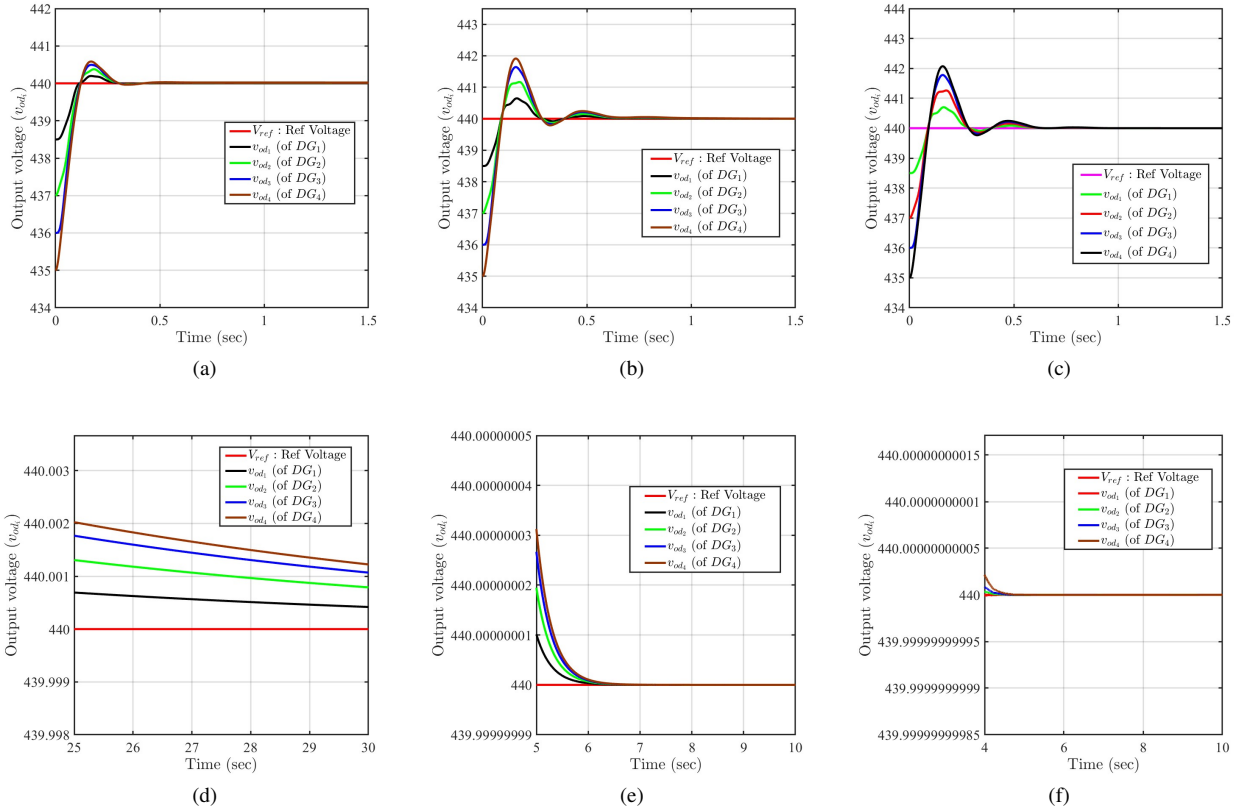

Fig. 6. (a) Output voltage (v_{od_i}) consensus profile of all four DGUs achieved by $\Xi_{c_1}(s)$; (b) Output voltage consensus achieved by $\Xi_{c_2}(s)$; (c) Output voltage consensus achieved by $\Xi_{c_3}(s)$; (d) Magnified version of the converging v_{od_i} trajectories achieved by $\Xi_{c_1}(s)$ during 25 sec $\leq t \leq$ 30 sec; (e) State of consensus during 5 sec $\leq t \leq$ 10 sec achieved by $\Xi_{c_2}(s)$; (f) State of consensus during 4 sec $\leq t \leq$ 10 sec achieved by $\Xi_{c_3}(s)$.

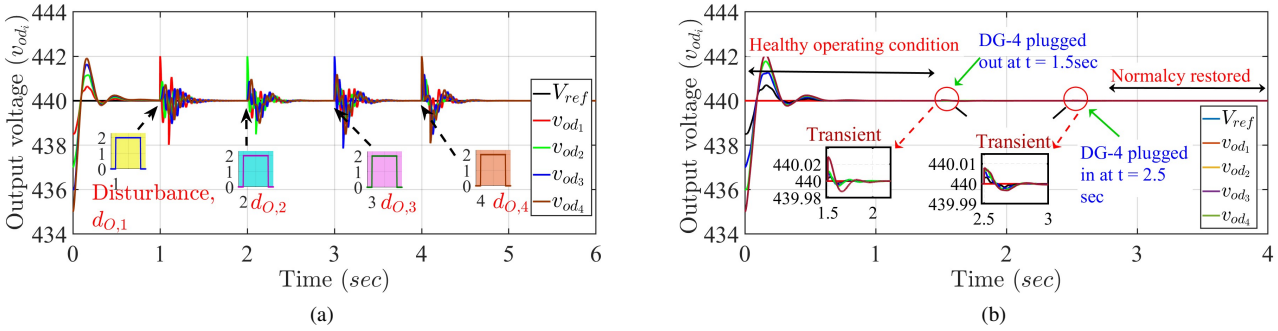

Fig. 7. (a) Output voltage (v_{od_i}) consensus profile of all four DGUs in presence of a pulse (output) disturbance injected to the DGs one by one; (b) Output voltage consensus profile of the DGUs when DGU-4 got plugged out at $t = 1.5$ sec and after sometime (at $t = 2.5$ sec), it plugged in.

network (i.e. plugged in) causing a similar bounded transient profile and decayed within 0.5 seconds. It shows that the strength of the SNI-based cooperative control scheme to sustain the plug-and-play operation.

Case 3: Impact of topology switching

The topologies 1, 2 and 3 shown in Fig. 5a, 5b, and Fig. 5c have been used to generate the voltage consensus profile during topology switching. The following sequence of topology variation $1 \rightarrow 2 \rightarrow 3 \rightarrow 1$ has been considered in the simulation. Fig. 8 depicts that the first switching occurred at $t = 2.5$ sec, followed by two more switching at $t = 2.5$ sec and $t = 3.5$ sec, respectively. The figure reports that the voltage fluctuations during the switching remain negligible, as small as 2% of the steady-state value, and decay quickly to zero within $0.5-0.6$ seconds, as illustrated by the zoomed portions of the graph. So, the simulation response study confirms that $\Xi_{c_3}(s)$ facilitates topology switching.

VI. Conclusion

This paper has proposed a new cooperative control scheme to solve the distributed secondary voltage control (DSVC)

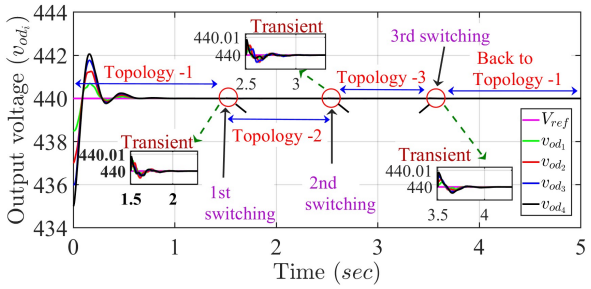

Fig. 8. (a) Output voltage (v_{od_i}) consensus response of all four DGUs due to changes in the network topology.

problem of AC microgrid(s) utilising the multi-agent NI approach. It suggests a distributed two-layer control scheme where the inner loop applies an input-output feedback linearisation technique to get a double-integrator (being NI) mapping of the voltage dynamics ($q_i \mapsto v_{od_i}$) of each DGU. While the outer loop executes a distributed SNI control law on the feedback-linearised DGUs to achieve the output voltage synchronisation among all the units. The theoretical proof exploits the eigenvalue loci technique in contrast to the complicated Lyapunov stability-based approaches [1], [5]–[8], etc., or the existing multi-agent NI-SNI stability results [9]–[11], [13], [17]. The proposed scheme has disturbance-attenuation capabilities and preserves the stability of the overall microgrid during critical phases like plug-and-play operation and topology switching. The paper also studies the suitable configurations of first-order and second-order distributed SNI controllers and compares their performance via extensive simulation studies. In future scopes, adaptive NI-based cooperative control schemes can be explored.

REFERENCES

[1] A. Bidram, A. Davoudi, F. L. Lewis, and J. M. Guerrero, "Distributed cooperative secondary control of microgrids using feedback linearization," *IEEE Transactions on Power Systems*, vol. 28, no. 3, pp. 3462–3470, 2013.

[2] A. Bidram, A. Davoudi, F. L. Lewis, and Z. Qu, "Secondary control of microgrids based on distributed cooperative control of multi-agent systems," *IET Generation, Transmission & Distribution*, vol. 7, no. 8, pp. 822–831, 2013.

[3] A. Bidram, F. L. Lewis, and A. Davoudi, "Distributed control systems for small-scale power networks: Using multiagent cooperative control theory," *IEEE Control Systems Magazine*, vol. 34, no. 6, pp. 56–77, 2014.

[4] J. W. Simpson-Porco, Q. Shafiee, F. Dörfler, J. C. Vasquez, J. M. Guerrero, and F. Bullo, "Secondary frequency and voltage control of islanded microgrids via distributed averaging," *IEEE Transactions on Industrial Electronics*, vol. 62, no. 11, pp. 7025–7038, May 2015.

[5] N. M. Dehkordi, N. Sadati, and M. Hamzeh, "Fully distributed cooperative secondary frequency and voltage control of islanded microgrids," *IEEE Transactions on Energy Conversion*, vol. 32, no. 2, pp. 675–685, 2017.

[6] H.-J. Yoo, T.-T. Nguyen, and H.-M. Kim, "Consensus-based distributed coordination control of hybrid ac/dc microgrids," *IEEE Transactions on Sustainable Energy*, vol. 11, no. 2, pp. 629–639, Feb 2019.

[7] Z. Wang, J. Wang, M. Ma, H. Yang, D. Chen, L. Wang, and P. Li, "Distributed event-triggered fixed-time fault-tolerant secondary control of islanded ac microgrid," *IEEE Transactions on Power Systems*, vol. 37, no. 5, pp. 4078–4093, Jan 2022.

[8] C. Zhang, X. Dou, X. Quan, Q. Hu, Z. Wu, and Y. Lv, "Distributed secondary control for island microgrids with expected dynamic performance under communication delays," *IEEE Transactions on Smart Grid*, vol. 14, no. 3, pp. 2010–2022, Oct 2023.

[9] J. Wang, A. Lanzon, and I. R. Petersen, "Robust output feedback consensus for networked negative-imaginary systems," *IEEE Transactions on Automatic Control*, vol. 60, no. 9, pp. 2547–2552, Sep 2015.

[10] J. Wang, A. Lanzon, and I. R. Petersen, "Robust cooperative control of multiple heterogeneous negative-imaginary systems," *Automatica*, vol. 61, pp. 64–72, 2015.

[11] V. P. Tran, M. A. Garratt, and I. R. Petersen, "Multi-vehicle formation control and obstacle avoidance using negative-imaginary systems theory," *IFAC Journal of Systems and Control*, vol. 15, pp. 1–23, March 2021.

[12] J. Hu, B. Lennox, and F. Arvin, "Robust formation control for networked robotic systems using negative imaginary dynamics," *Automatica*, vol. 140, no. 110235, pp. 1–9, June 2022.

[13] C. Li, J. Wang, J. Shan, A. Lanzon, and I. R. Petersen, "Robust cooperative control of networked train platoons: A negative-imaginary systems' perspective," *IEEE Transactions on Control of Network Systems*, vol. 8, no. 4, pp. 1743–1753, Dec 2021.

[14] Y. Su, P. Bhowmick, and A. Lanzon, "Cooperative control of multi-agent negative imaginary systems with applications to UAVs, including hardware implementation results," in *Proceedings of the 2023 European Control Conference*, June 2023, pp. 1–6.

[15] ——, "A negative imaginary theory-based time-varying group formation tracking scheme for multi-robot systems: Applications to quadcopters," in *Proceedings of the 2023 IEEE International Conference on Robotics and Automation*, May-June 2023, pp. 1435–1441.

[16] P. Bhowmick, A. Ganguly, and S. Sen, "A new consensus-based formation tracking scheme for a class of robotic systems using negative imaginary property," *IFAC-PapersOnLine*, vol. 55, no. 1, pp. 685–690, 2022.

[17] K. Shi, I. R. Petersen, and I. G. Vladimirov, "Output feedback consensus for networked heterogeneous nonlinear negative-imaginary systems with free body motion," *IEEE Transactions on Automatic Control*, vol. 68, no. 9, pp. 5536–5543, Sep 2023.

[18] D. Abara, P. Bhowmick, and A. Lanzon, "A negative imaginary robust formation control scheme for networked multi-tilt tricopters utilizing an inner-loop sliding-mode control technique," *Automatica*, vol. 169, no. 111813, pp. 1–15, July 2024.

[19] A. Lanzon and I. R. Petersen, "Stability robustness of a feedback interconnection of systems with negative imaginary frequency response," *IEEE Transactions on Automatic Control*, vol. 53, no. 4, pp. 1042–1046, May 2008.

[20] A. Lanzon and P. Bhowmick, "Characterisation of input-output negative imaginary systems in a dissipative framework," *IEEE Transactions on Automatic Control*, vol. 68, no. 2, pp. 959–974, Feb 2023.

[21] P. Bhowmick and A. Lanzon, "Dynamic dissipative characterisation of time-domain input-output negative imaginary systems," *Automatica*, vol. 164, no. 111620, pp. 1–14, June 2024.

[22] O. Skeik, J. Hu, F. Arvin, and A. Lanzon, "Cooperative control of integrator negative imaginary systems with application to rendezvous multiple mobile robots," in *Proceedings of 12th International Workshop on Robot Motion and Control*, Poznan, Poland, July 2019, pp. 15–20.

[23] P. Bhowmick and S. Patra, "On decentralized integral controllability of stable negative-imaginary systems and some related extensions," *Automatica*, vol. 94, pp. 443–451, Aug 2018.

[24] M. A. Mabrok, A. G. Kallapur, I. R. Petersen, and A. Lanzon, "Generalizing negative imaginary systems theory to include free body dynamics: Control of highly resonant structures with free body motion," *IEEE Transactions on Automatic Control*, vol. 59, no. 10, pp. 2692–2707, Oct 2014.

[25] A. Lanzon and H.-J. Chen, "Feedback stability of negative imaginary systems," *IEEE Transactions on Automatic Control*, vol. 62, no. 11, pp. 5620–5633, Nov 2017.

[26] F. L. Lewis, H. Zhang, K. Hengster-Movric, and A. Das, *Cooperative control of multi-agent systems: Optimal and adaptive design approaches*, 1st ed. Springer-Verlag London, 2014.

[27] J. J. Belletrutti and A. G. J. MacFarlane, "Characteristic loci techniques in multivariable-control-system design," *Proceedings of the Institution of Electrical Engineers*, vol. 118, no. 9, pp. 1291–1297, Sep 1971.

[28] A. G. J. Macfarlane and J. J. Belletrutti, "The characteristic locus design method," *Automatica*, vol. 9, no. 5, pp. 575–588, 1973.

[29] N. Pogaku, M. Prodanovic, and T. C. Green, "Modeling, analysis and testing of autonomous operation of an inverter-based microgrid," *IEEE Transactions on Power Electronics*, vol. 22, no. 2, pp. 613–625, 2007.